Electronic Supplementary Material (ESI) for Journal of Materials Chemistry B.

Supporting information

Magnetic mesoporous silica/ε-polylysine nanomotor-based removers of blood Pb^{2+}

Zhiyong Liu,‡[a] Tingting Xu,‡[a, b] Meng Wang,[a] Chun Mao*[a] and Bo Chi *[c]

[a] National and Local Joint Engineering Research Center of Biomedical Functional Materials, Jiangsu Key Laboratory of Biofunctional Materials, School of Chemistry and Materials Science, Nanjing Normal University, Nanjing 210023, China

[b] Jiangsu Co-Innovation Center of Efficient Processing and Utilization of Forest Resources, College of Light Industry and Food Engineering, Nanjing Forestry University, Nanjing 210037, China

[c] State Key Laboratory of Materials-Oriented Chemical Engineering, College of Food Science and Light Industry, Nanjing Tech University, Nanjing 211816, China

Adsorption kinetics tested in aqueous condition

For adsorption kinetics study, 10 mg of MMS/P NRs were added to 10 mL aqueous solutions with Pb^{2+} concentration of 100 ppm. The adsorption process was carried out in water bath device with a constant temperature of 37°C. The adsorbents were removed from the solution using a magnet at prescribed times (10 min, 30 min, 1 h, 2 h, 4 h, 8 h, 12 h, 16 h, 20 h, 24 h). The concentrations of the heavy metal ions were detected by ICP method.[1]

Activated partial thromboplastin time (APTT), prothrombin time (PT) and thrombin time (TT) test

The platelet poor plasma (PPP) was obtained by centrifugation. Then 20 mg mL^{-1} of adsorbents were incubated in 1.5 mL PPP at 37°C for 1 h, followed by measuring the coagulation times including APTT, PT and TT with a Rayto-2204C Semi automated coagulometer (USA). All the tests were performed in triplicate.[2]

Complement activation

MMS/P NRs were incubated with PPP obtained by centrifugation from whole blood at 37°C for 20 min. Then the cleavage of complement component C3 was monitored by detecting the formation of its activation peptides, C3a and C3a des-Arg, using a commercial C3a Elisa kit (BD OptEIA™) with a microplate reader (Biotek Synergy2, USA) according to the manufacturer's instructions.[3]

Adsorption isotherms tested in aqueous condition

The adsorption isotherm study was carried out by exposing 10 mg of MMS/P NRs to 10 mL aqueous solutions with different initial ion concentrations ranging from 1 to 100 ppm for 24 h at 37°C, respectively. The adsorbents were also removed from the solution using a magnet. In order to determine the adsorbed amount of Pb^{2+}, the

concentrations of Pb^{2+} in the solution were detected before and after adsorption by using the ICP method.[4]

The adsorption data were dealt with the pseodo-first-order, the pseudo-second-order and the intraparticle diffusion models.[5]

The pseodo-first-order model was described as bellow:

$$\ln(q_e - q_t) = \ln q_e - k_1 t \quad (1)$$

the pseudo-second-order order model was shown as bellow:

$$\frac{t}{q_t} = \frac{1}{k_2 q_e^2} + \frac{t}{q_e} \quad (2)$$

and the intraparticle diffusion was shown as bellow:

$$q_t = k_{diff}\sqrt{t} + c \quad (3)$$

where q_t and q_e (mmol g^{-1}) represented the amount of Pb^{2+} adsorbed on the adsorbents at time t (min) and equilibrium, respectively. k_1, k_2 and k_{diff} were the rate constants for each kinetic model.

Both Langmuir and Freundlich adsorption isotherms were obtained under 25°C.[6]

The Langmuir adsorption isotherms was described as bellow:

$$\frac{C_e}{q_e} = \frac{C_e}{q_{max}} + \frac{1}{K_L q_{max}} \quad (1)$$

and the Freundlich adsorption isotherms was shown as bellow:

$$\ln q_e = \ln K_F + \frac{1}{n} \ln C_e \quad (2)$$

where q_e and q_{max} represented the equilibrium and maximum Pb^{2+} adsorption (mg g^{-1}), C_e meant the equilibrium Pb^{2+} concentration in solution (mg L^{-1}), K_L was the Langmuir constant and increased with the affinity of sorbent for the sorbate. q_{max}

represented the maximum adsorption capacity (mg g^{-1}) of the sorbent. K_F and n represented constants and favorable adsorptions occur when n was greater than 1.

Hemolysis tests

2% red blood cells (RBCs) suspension was added to MMS/P NRs which were weighed and immerged in saline water for 24 h.[7] Meanwhile, the RBCs were also incubated with PBS and twice-distilled water as negative control and positive control, respectively. After 1 h incubation, samples were centrifuged for 10 min at 1500 rpm. The optical density of the supernatant was measured at 545 nm. The percent hemolysis was calculated as follows.

$$\text{Percent hemolysis}(\%) = \left(\frac{\text{sample absorbance} - \text{negative control absorbance}}{\text{positive control absorbance} - \text{negtive control absorbance}} \right) \times 100$$

The morphological changes of RBCs were observed and photographed with an Olympus E-620 camera (Olympus Ltd., Japan).[8]

Routine blood analytes

The routine blood analytes were carried out before and after the blood was incubated with the MMS/P NRs.

Immune inflammatory system changes

Interleukin-6 (il-6), tumor necrosis factor-α (TNF-α) and C-reactive protein (crp) are nonspecific pro-inflammatory factors and sensitive markers of inflammatory reaction.[9] In this work, they were detected by Elisa kit (BD OptEIA™) with a microplate reader (Biotek Synergy2, USA) according to the manufacturer's instructions. Furthermore, in order to further study the peripheral blood lymphocyte

immunity, the proportion of $CD3^+CD4^+/CD3^+CD8^+$ cells were calculated by flow cytometer (BD FACSCalibur, USA).[10]

The selective adsorption of haemoglobin(Hb) test

Prepare 2 mg mL^{-1} Hb solution with the Pb^{2+} concentration of 1 ppm, and silent mix for 60 min. 10 mg mL^{-1} MMP/NRs were used to adsorb clean Hb and Pb^{2+}-contaminated Hb in a variable magnetic field for 30 min, then magnetically separate. The absorbance at 280 nm of the supernatant was measured.

Determination of optimal adsorption conditions

We used different concentrations of MMS/P NRs to adsorb 0.6 ppm Pb^{2+} solution and then determined the adsorption efficiency of Pb^{2+}, detected the adsorption efficiency of different origin concentration of Pb^{2+} solution with 10 mg mL^{-1} MMS/P NRs, and tested the adsorption efficiency of 10 mg mL^{-1} MMS/P NRs for 0.6 ppm Pb^{2+} solution at different times to obtain the best experimental conditions.

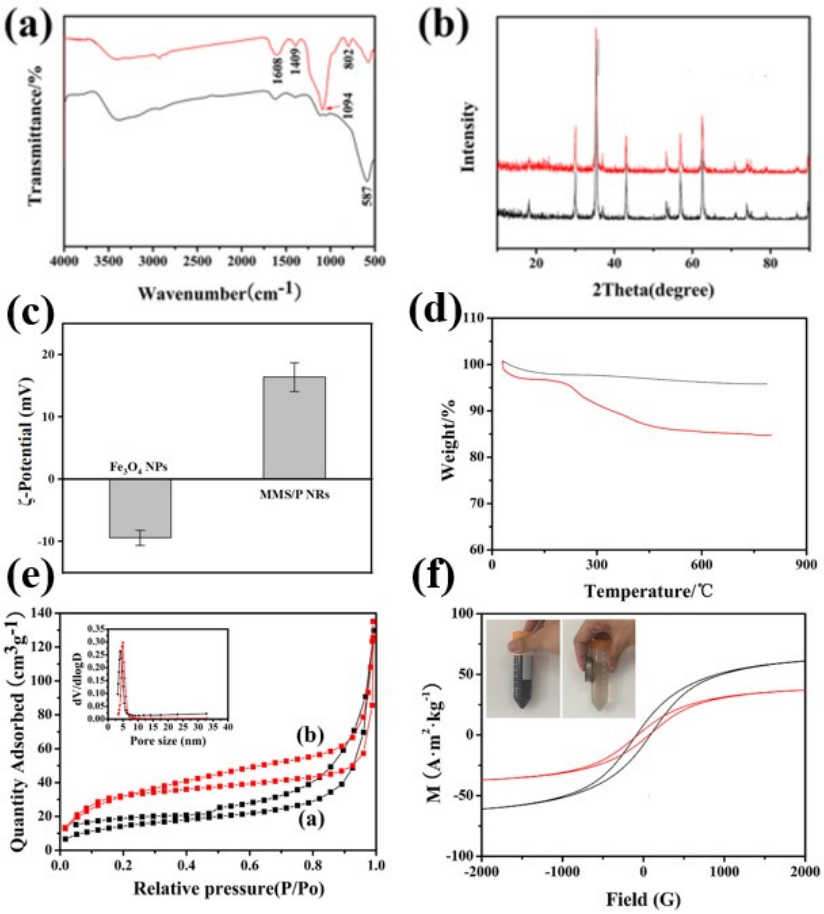

Fig. S1. (a) FT-IR spectra of Fe_3O_4 and MMS/P NRs; (b) the XRD spectra of Fe_3O_4 and MMS/P NRs; (c) ζ -potential of Fe_3O_4 NPs and MMS/P NRs; (d) TGA profiles of Fe_3O_4 (black) and MMS/P NRs (red); (e) nitrogen adsorption-desorption isotherms and pore size distribution (inset) of MMS/P NRs before (black) and after (red) removal of the template, and (f) the hysteresis loops of Fe_3O_4 NPs (black) and MMS/P NRs (red).

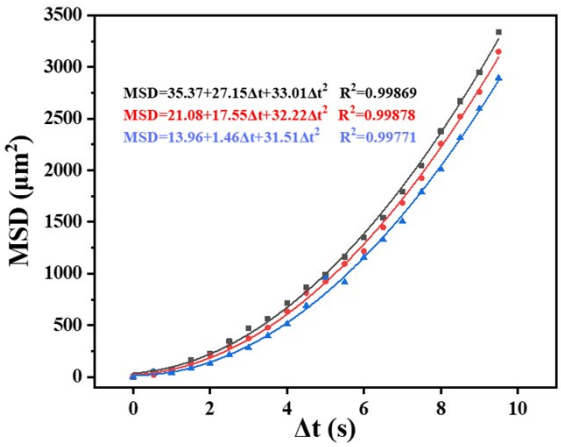

Fig. S2. The mean square displacement of MMS/P NRs in aqueous solution.

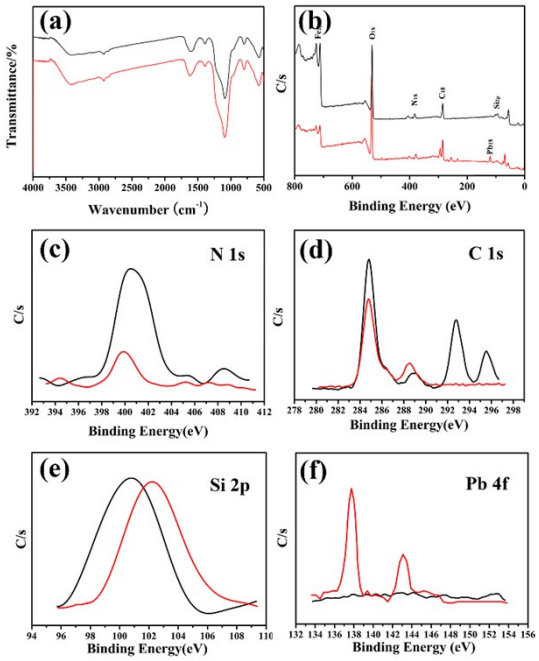

Fig. S3. (a) FT-IR spectra of the MMS/P NRs before (black) and after (red) adsorption; (b) the XPS images of the MMS/P NRs before (black) and after (red) Pb^{2+} adsorption process (water phase); and the partial enlarged XPS images of (c) N1s, (d) C1s, (e) Si 2p and (f) Pb 4f of the MMS/P NRs before (black) and after (red) Pb^{2+} adsorption process (water phase).

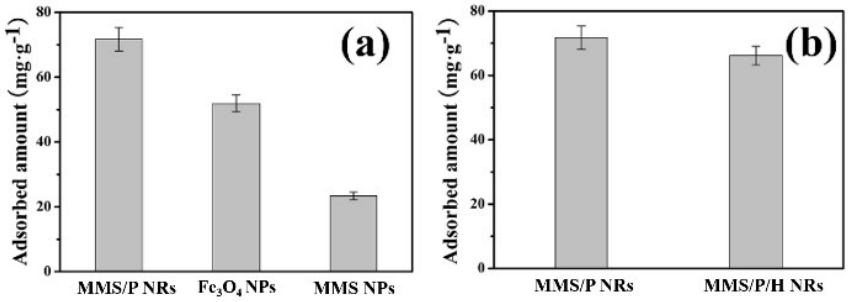

Fig. S4. Adsorption performance of Pb^{2+} on (a) different samples and (b) before (MMS/P NRs) and after (MMS/P/H NRs) modification of heparin.

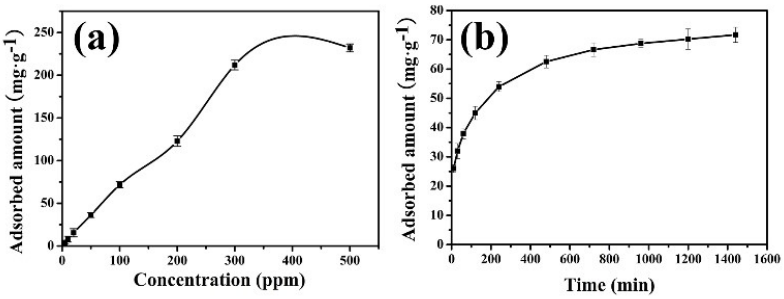

Fig. S5. (a) Adsorption performance of Pb^{2+} by MMS/P NRs under different concentration of Pb^{2+} (adsorption time was 24 h); (b) adsorption performance for different time (adsorption concentration was 100 ppm).

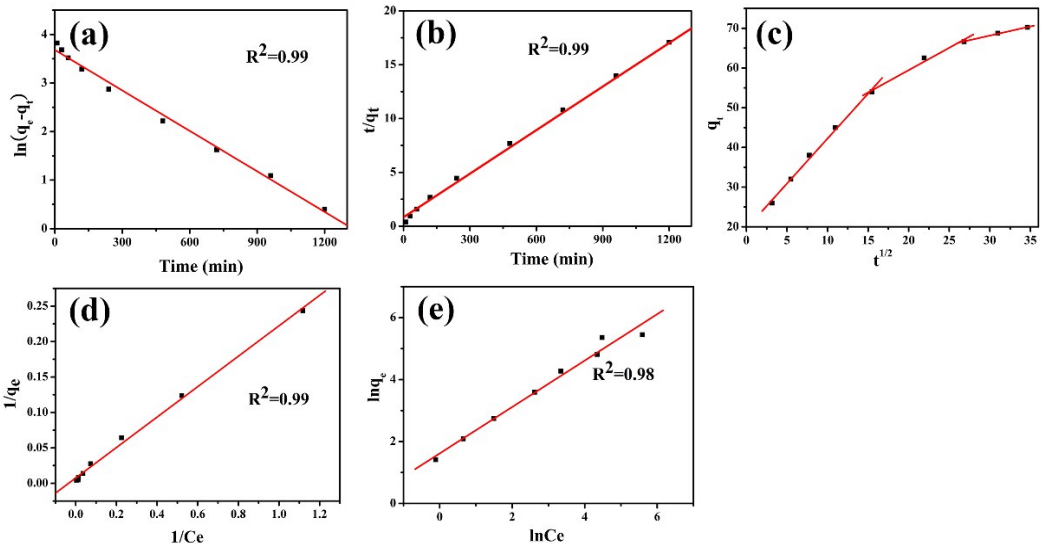

Fig. S6. (a) Pseudo-first-order kinetic model plots, (b) pseudo-second-order kinetic model plots and (c) intraparticle diffusion kinetics for the adsorption of Pb^{2+} on the MMS/P NRs; (d) Langmuir and (e) Freundlich adsorption isotherms for the adsorption of Pb^{2+} on the MMS/P NRs.

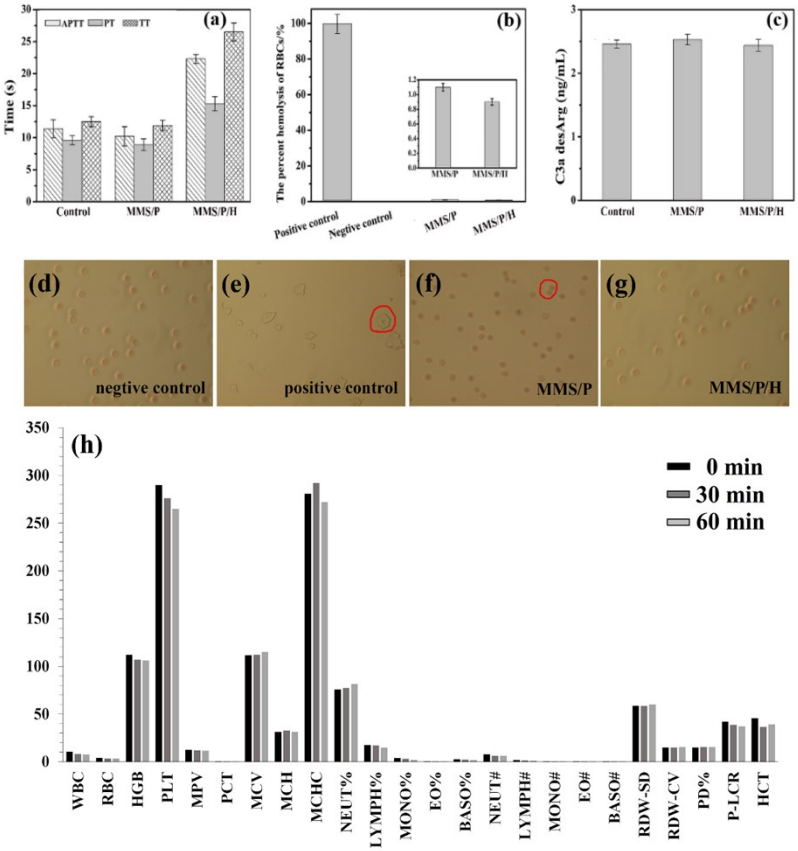

Fig. S7. (a) APTT/PT/TT values, (b) the hemolysis ratio and (c) the concentration of C3a desArg of MMS/P NRs before and after soaking in heparin solution; optical images of RBCs treated by (d) negative control, (e) positive control (f) MMS/P NRs and (g) MMS/P/H NRs; (h) the routine blood results of the MMS/P NRs.

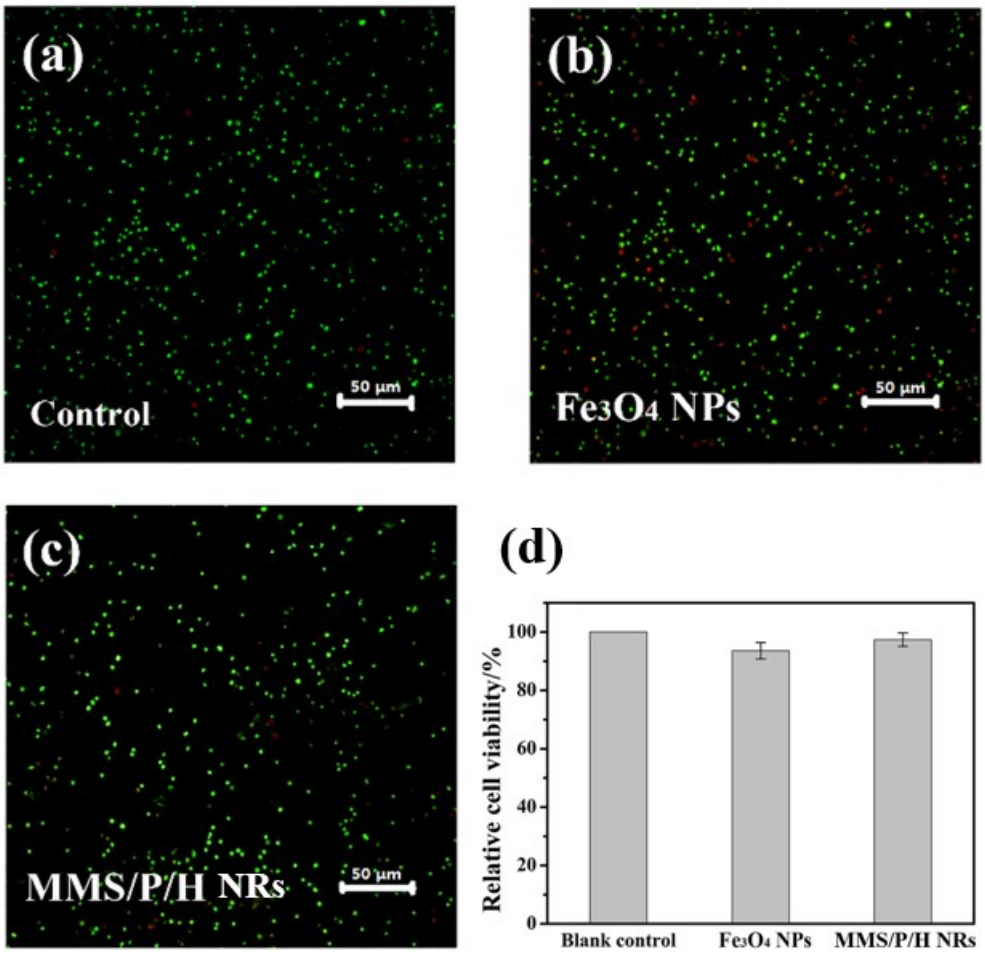

Fig. S8. Fluorescence confocal images of inside peripheral blood lymphocyte before (a) and after being incubated with (b) Fe_3O_4 NPs and (c) the MMS/P/H NRs; (d) cell viability of peripheral blood lymphocyte before and after being incubated with Fe_3O_4 and the MMS/P/H NRs.

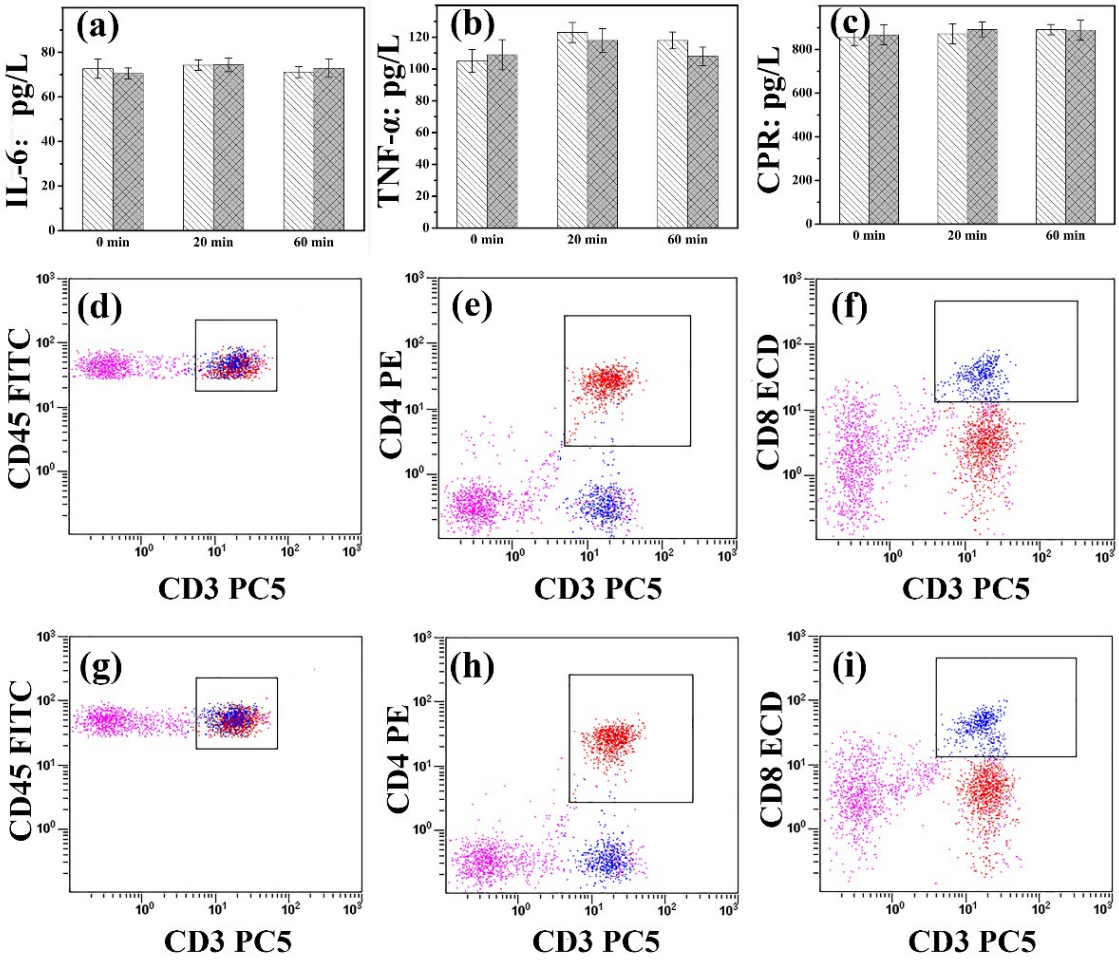

Fig. S9. The inflammatory factor (a) IL-6, (b) TNF-α and (c) CRP levels before and after adsorption for different times; effect on cellular immunity and inflammation before and after adsorption by MMS/P/H NRs: (d, e, f) displayed the cellular antigen expression levels of $CD3^+$ $CD45^+$, $CD3^+$ $CD4^+$, $CD3^+$ $CD8^+$ before adsorption, while (g, h, i) showed those levels after adsorption.

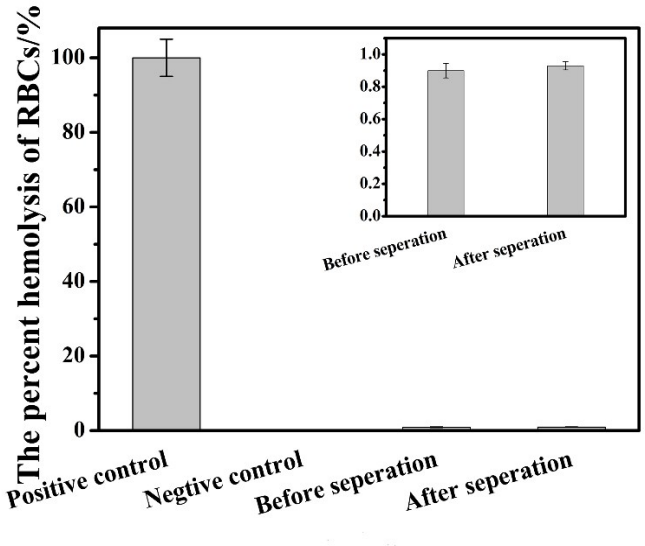

Fig. S10. The hemolysis ratio of RBCs before and after MMS/P/H NPs being magnetic seperation.

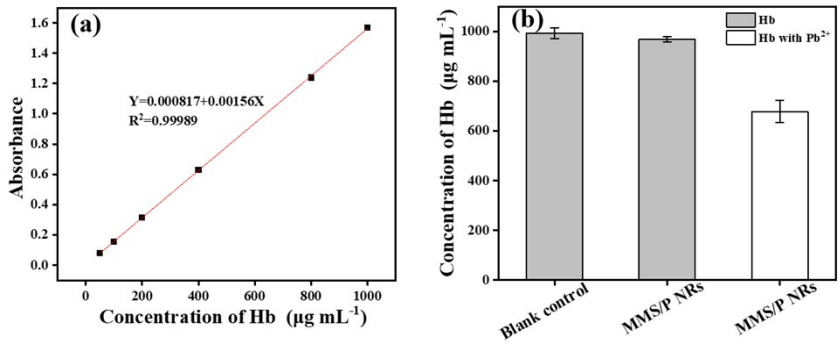

Fig. S11. (a) Standard concentration curve of Hb. (b) MMS/P NRs selectively adsorb Hb contaminated with Pb^{2+}.

Table S1. Summary of current research of the blood Pb^{2+} absorbent

Materials	Autonomous movement	Adsorption environment	Adsorption mechanism	Ref.
Pb^{2+}-bound 1	×	Blood	Magnetic nanomaterials were coated with fluorescent receptors to detect and remove Pb^{2+}	11
Fe_3C-(PEI-DTPA)$_n$	×	Blood	Heavy-metal binding EDTA-like Chelators modified magnetic nanoparticles for the adsorption and separation of Pb^{2+}	12
C/Fe_3C-PEI-IDA	×	Blood	Nanomagnets coated with poly(ethylene imine) -iminodiacetic acid were used for specific adsorption of Pb^{2+} and separated from blood	13
SH-SBA-15	×	Blood and bile	MPTMS ((3-mercaptopro-Pyl) trimethoxysilane) Thiol-groups were used to modify mesoporous silica, and Pb^{2+} are absorbed by -SH on the surface of material	14
Fe_3O_4@SiO_2@DMSA	×	Blood and urine	Fe_3O_4@SiO_2 modified with the Meso-2,3-Dimercaptosuccinic acid and -SH was used to capture Pb^{2+} in blood and urine	15
MNP@DMSA	×	Blood, RBCs and plasma	Magnetic nano capture agent coated with the Meso-2, 3-Dimercaptosuccinic acid, and -SH was used to capture Pb^{2+}	16
Fe_3O_4 @ Au@DNA	×	Blood	Core-shell structured magnetic microspheres functionalized with the Pb^{2+}-binding aptamer as adsorbent, isolate and detect trace Pb^{2+}	17
$CaCO_3$ NDs	×	Blood	Construct “cyborg erythrocytes” through the in situ reaction of exogenous calcium and carbonate ions to generate calcium carbonate nanodots inside erythrocytes can remove Pb^{2+} in blood poisoning model	18
Bac@Ceria	√	Blood and organs	Non-pathogenic bacteria are decorated with cerium oxide nanoparticles and adsorb excessive Pb^{2+} in blood and organs	19
MMS/H	×	Blood and RBCs	Hemoglobin containing Pb^{2+} is selectively captured by hyperbranched poly(amidoamine)s, and magnetic separate from blood	20
$SrTiO_3$ NPs	×	Blood and urine	Pb^{2+} in water-soluble medium was enriched by physical adsorption of strontium titanate nanoparticles ($SrTiO_3$)	21

MMS/P NRs	√	Blood and RBCs	MMS/P NRs move autonomously under the guidance of magnetic field, capturing many Pb^{2+}-contaminated hemoglobin and fixing it in the mesoporous area, which was separated from blood by magnetic field	This work

Table S2. Specific surface, pore diameter and pore volume of MMS/P NRs and MMS NPs.

Sample	**Specific surface area (m^2 g^{-1})**	**Pore diameter (nm)**	**Pore volume (cm^3 g^{-1})**
MMS/P NRs	118.56	9.4	0.108
MMS NPs	303.34	10.8	0.306

Table S3. Pseudo-first order, pseudo-second order and intraparticle diffusion kinetic model parameters.

Heavy metal ions	**Pseudo-first-order kinetic**		**Pseudo-second-order kinetic**		**Intraparticle diffusion kinetic**	
	K_1	R_1	K_2	R_2	K_{diff}	R_{diff}
Pb^{2+}	$2.8*10^{-3}$	0.99	$2.5*10^{-4}$	0.99	2.27	0.99
					1.13	0.98
					0.46	0.99

Table S4. Langmuir and Freundlich adsorption isothermal constants, correlation coefficients.

Heavy metal ions	**Langmuir**			**Freundlich**		
Pb^{2+}	q_{max}	K_L	R^2	n	K_F	R^2
	131.58	0.0354	0.99	1.34	5.04	0.98

Table S5. The efficiency of Pb^{2+} adsorption in the aqueous condition.

adsorbent/mg·mL^{-1}	**adsorption efficiency/%**	**adsorption time/min**	**adsorption efficiency/%**	**Pb^{2+}/ppm**	**adsorption efficiency/%**
1	31.72	**10**	26.61	**0.6**	65.87
2	43.98	**30**	65.87	**1**	63.35
5	57.39	**45**	66.57	**2**	43.04
10	65.87	**60**	66.38	**5**	34.19
20	68.87	**90**	67.29	**10**	33.46
50	70.26	\	\	\	\

Table S6. The bond length and bond dissociation energy of Pb^{2+} bound with ε-PL.

	Pb-N14	Pb-N3	Pb-O2	N3-Pb-N14	N14-Pb-O2
Bond length (Å)	2.35	2.48	2.07	N3-Pb 2.45 N14-Pb 2.41	O2-Pb 2.20 N14-Pb 2.41
Bond dissociation energy (kJ mol^{-1})	149.05	132.65	157.03	203.03	156.16

Table S7. Comparison of HOMO-LUMO transition energies between Pb^{2+} and ε-PL.

	HOMO(Hartree)	**LUMO(Hartree)**	**E_{gap}(Hartree)**
Pb-N14	-0.28462	-0,14491	0.13971
Pb-N3	-0.27543	-0.15518	0.12025
Pb-O2	-0.27414	-0.13345	0.14069
N3-Pb-N14	-0.32621	-0.1058	0.22041
N14-Pb-O2	-0.29938	-0.1112	0.18818

Reference

(1) S. M. Ponder, J. G. Darab and T. E. Mallouk, Environ. Sci. Technol., 2000, 34, 2564-2569.

(2) H. Chen, M. F. Neerman, A. R. Parrish and E. E. Simanek, J. Am. Chem. Soc., 2004, 126, 10044-10048.

(3) M. M. Wan, Y. Y. Li, T. Yang, T. Zhang, X. D. Sun and J. H. Zhu, Chem. Eur. J., 2016, 22, 6294-6301.

(4) G. Zhao, J. Li, X. Ren, C. Chen and X. Wang, *Environ. Sci. Technol.,* 2011, **45,** 10454-10462.

(5) H. Lu, W. Zhang, Y. Yang, X. Huang, S. Wang and R. Qiu, *Water Res.,* 2012, **46,** 854-862.

(6) S. Y. Liu, J. Gao, Y. J. Yang, Y. C. Yang and Z. X. Ye, *J. Hazard. Mater.,* 2010, **173,** 558-562.

(7) R. K. Kainthan, J. Janzen, E. Levin, D. V. Devine and D. E. Brooks, *Biomacromolecules,* 2006, **7,** 703-709.

(8) F. Peng, H. Li, D. Wang, P. Tian, Y. Tian,; G. Yuan, D. Xu and X. Liu, *ACS Appl. Mater. Interfaces,* 2016, **8,** 35033-35044.

(9) V. Panichi, M. Migliori, S. De Pietro, D. Taccola, B. Andreini, M. R. Metelli, L. Giovannini and R. Palla, *Kidney Int.,* 2000, **76,** S96-103.

(10) A. Naji, S. Le Rond, A. Durrbach, I. Krawice-Radanne, C. Creput, M. Daouya, J. Caumartin, J. LeMaoult, E. D. Carosella and N. Rouas-Freiss, *Blood,* 2007, **110,** 3936-3948.

(11) H. Y. Lee, D. R. Bae, J. C. Park, H. Song, W. S. Han and J. H. Jung, *Angew. Chem.*

Int. Ed., 2009, **48,** 1239-1243.

(12) I. K. Herrmann, M. Urner, F. M. Koehler, M. Hasler, B. Roth-Z'graggen, R. N. Grass, U. Ziegler and B. Beck-Schimmer, W. J. Stark, *Small*, 2010, **6**, 1388-1392.

(13) I. K. Herrmann, A. Schlegel, R. Graf, C. M. Schumacher, N. Senn, M. Hasler, S. Gschwind, A. M. Hirt, D. Gunther, P. A. Clavien, W. J. Stark and B. Beck-Schimmer, *Nanoscale*, 2013, **5**, 8718-8723.

(14) W. Huang, P. Zhang, H. Xu, S. Chang, Y. He, F. Wang and G. Liang, *Nanotechnology*, 2015, **26**, 385101.

(15) Y. Xiang, Z. Bai, S. Zhang, Y. Sun, S. Wang, X. Wei, W. Mo, J. Long, Z. Liu, C. Yang, L. Zheng, X. Guo, W. Xiaoyang, F. Mao and N. Feng, *Nanomed.-Nanotechnol.*, 2017, **13**, 1341-1351.

(16) X. Guo, W. Wang, X. Yuan, Y. Yang, Q. Tian, Y. Xiang, Y. Sun and Z. Bai, *J. Colloid Interf. Sci.*, 2019, **536**, 563-574.

(17) Y. K. Li, W. T. Li, X. Liu, T. Yang, M. L. Chen and J. H. Wang, *Talanta*, 2019, **203**, 210-219.

(18) X. Ru, Y. Guo, Z. Bai, X. Xie, X. Ma, L. Zhu, K. Wang, F. Wang, L. Yang and J. Lu, *Commun. Chem.*, 2019, **2**, 105.

(19) P. Pan, J. X. Fan, X. N. Wang, J. W. Wang, D. W. Zheng, H. Cheng and X. Z. Zhang, *Adv. Sci.*, 2019, **6**, 1902500.

(20) M. M. Wan, T. T. Xu, B. Chi, M. Wang, Y. Huang, Q. Wang, T. Li, W. Q. Yan, H. Chen, P. Xu, C. Mao, B. Zhao, J. Shen, H. Xu and D. Q. Shi, *Angew. Chem. Int. Ed.*, 2019, **58**, 10582-10586.

(21) W. I. Mortada and A. M. Abdelghany, Biol. *Trace Elem. Res.*, 2020, **193**, 100-110.